AD-A281 683

‖‖‖‖‖‖‖‖‖‖‖‖‖‖‖‖

①

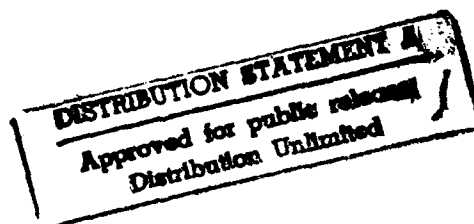# NASA ICASE

# NUMERICAL SIMULATION OF TWO-DIMENSIONAL SPATIALLY-DEVELOPING MIXING LAYERS

DTIC
S ELECTE
JUL 1 4 1994
B D

R. V. Wilson
A. O. Demuren

DISTRIBUTION STATEMENT A
Approved for public release
Distribution Unlimited

DTIC QUALITY INSPECTED 5

uSPf  94-21568

‖‖‖‖‖‖‖‖‖‖‖‖‖‖‖‖

USRA  Operated by Universities Space Research Association

94  7  12  261

# ICASE Fluid Mechanics

Due to increasing research being conducted at ICASE in the field of fluid mechanics, future ICASE reports in this area of research will be printed with a green cover. Applied and numerical mathematics reports will have the familiar blue cover, while computer science reports will have yellow covers. In all other aspects the reports will remain the same; in particular, they will continue to be submitted to the appropriate journals or conferences for formal publication.

# NUMERICAL SIMULATION OF TWO-DIMENSIONAL

# SPATIALLY-DEVELOPING MIXING LAYERS

*R. V. Wilson*[1] *and A. O. Demuren*
Department of Mechanical Engineering
Old Dominion University
Norfolk, VA 23529

## ABSTRACT

Two-dimensional, incompressible, spatially developing mixing layer simulations are performed at $Re = 10^2$ and $10^4$ with two classes of perturbations applied at the inlet boundary; (*i*) combinations of discrete modes from linear stability theory, and (*ii*) a broad spectrum of modes derived from experimentally measured velocity spectra. The effect of the type and strength of inlet perturbations on vortex dynamics and time-averaged properties are explored. Two-point spatial velocity and autocorrelations are used to estimate the size and lifetime of the resulting coherent structures and to explore possible feedback effects. The computed time-averaged properties such as mean velocity profiles, turbulent statistics, and spread rates show good agreement with experimentally measured values. It is shown that by forcing with a broad spectrum of modes derived from an experimental energy spectrum many experimentally observed phenomena can be reproduced by a 2-D simulation. The strength of the forcing merely affected the length required for the dominant coherent structures to become fully-developed. Thus intensities comparable to those of the background turbulence in many wind tunnel experiments produced the same results, given sufficient simulation length.

# I. INTRODUCTION

Mixing layers are studied extensively because of their wide practical applications as well as for scientific interest. Apart from the obvious cases of two stream mixing layers and the near field of jets they can be found in most shear flows away from walls. Many complicated flow situations can be shown to be a synthesis of wall boundary layers and mixing layers, amongst others. Thus, even in recirculating flows, mixing layers play an important role and their understanding is necessary for the prediction of many practical flow situations. Of the two major flow types: the wall boundary layer and the free mixing layer, the latter is the less understood, more controversial and less predictable.

A few of the major controversies are the importance of coherent structures in free shear flows, their dimensionality and their relationship to real turbulence. Following Brown and Roshko[1]'s landmark study on the dominant role of coherent structures in the evolution of mixing layers, and their persistence even at high Reynolds numbers, several experimental investigations[2-8] have been performed to explore the role of the coherent structures, the mechanisms for their formation and their eventual breakdown into random turbulent motion. Winant and Browand[2] observed that the process of vortex pairing was responsible for shear layer growth. This was essentially a two-dimensional process. Dimotakis and Brown[3] confirmed the persistence of the coherent structures at high Reynolds numbers and that large-scale entrainment and small-scale mixing occurred through distinct processes at different stages of evolution of the coherent structures. Ho and Huang[4] studied mixing layers perturbed with disturbances of different frequencies. They found that vortex pairing was controlled by the presence of subharmonic modes of the fundamental frequency of the mixing layer. Thus vortex mergings at specific locations involving a desired number of vortices could be initiated simply by forcing the layer with disturbances which contain corre-

1

sponding subharmonic modes. Later results by Ho et al.[5] have downplayed the ability to control this process because phase jitter could lead to decorrelation between the fundamental and its sub-harmonic modes leading to more random merging locations. Perhaps the major challenge to the Brown and Roshko picture of the role of coherent structures was presented by Chandrsuda et al.[6]. Based on the analysis of their experimental data, they postulated that this must be a relic of the transition process and that the spanwise vortices would only be dominant in the absence of initially turbulent boundary layers at the splitter plate, high free stream turbulence, or finite three-dimensional disturbances. This assertion was partly confirmed by Browand and Latigo[7] in their study of a plane mixing layer, but other studies such as that by Hussain and Zaman[8] contradict this finding.

It is now believed[3] that a feedback mechanism could produce a disturbance, with a frequency related to the size of the domain, which would interact with the mixing layer to influence the development all the way to the inlet. Thus, the mixing layer could never forget its origin and self-similarity conditions would not exist. In a comprehensive review of experimental data of single stream mixing layers developing from different initial conditions, Birch[9] found that for turbulent initial conditions the spread rate in the developing region could overshoot the asymptotic value in the fully-developed region by over 20%, whereas with laminar initial conditions the spread rate monotonically increased to its asymptotic value with no associated overshoot. The author also found that for turbulent initial conditions, the turbulent shearing stress gradually approached the far-field, asymptotic value, while with laminar initial conditions an overshoot twice the asymptotic value of the turbulent shearing stress occurred. Bradshaw[10] reported the persistence of initial conditions up to 1000 initial momentum thicknesses in the mixing region of a round jet.

Linearized stability theory has been successful in predicting the initial development of the shear layer before the onset of vortex interactions which are in general strongly nonlinear. Michalke[11] performed a temporal stability analysis of a single plane mixing layer, which showed a finite band of wavenumbers experiencing exponential growth rates. All modes experienced constant phase speed independent of wavenumber. A stability analysis of the spatially-developing plane mixing layer was performed by Michalke[12], and Monkewitz and Huerre[13], with the latter considering both the Blasius and hyperbolic tangent velocity profiles of arbitrary velocity ratio. For both velocity profiles it was found that the maximum spatial growth rate was approximately proportional to the velocity ratio, with a finite range of frequencies that experienced exponential growth rates. The phase velocity was found to be a function of frequency, with frequencies less than the most amplified mode experiencing a larger phase speed. The phase speed was approximately constant and equal to that predicted by temporal analysis for modes greater than the most amplified mode. It was found that linearized stability theory applied to a *spatially* developing mixing layer yielded growth rates which showed better agreement with experimental values.

Linear theory is not capable of predicting strongly nonlinear behavior such as saturation of the growth rates, suppression of one mode by another, and interaction of two or more vortices. The above mentioned phenomena must be simulated numerically. Riley and Metcalfe[14] performed 2-D and 3-D temporally-developing mixing layer simulations and found that when forced with a broad range of modes plus the fundamental mode at strong amplitudes, the shear layer exhibited larger initial growth rates followed by suppressed growth rates compared to simulations forced with only a broad range of modes. Cain et al.[15] studied the temporally-developing mixing layer and noted that by forcing the initial conditions with fluctuations at relatively high intensity, the initial growth rate was two to three times the asymptotic value. It was also found that the growth

of the momentum thickness was accelerated by concentrating the energy of the initial conditions in the most amplified band of wavenumbers predicted by linear theory. Corcos and Sherman[16] performed two-dimensional (2-D), time-developing mixing layer simulations and reported that the resulting vortex dynamics were largely determined by the subharmonic frequency content in the initial conditions. With only the fundamental mode present in the initial conditions, the initially uniform vortex sheet of the shear layer rolled up into an array of spanwise vorticity "lumps" separated by a distance of one fundamental wavelength. The addition of a subharmonic mode in phase with that of the fundamental mode resulted in two spanwise vorticity lumps merging to form a single larger structure which caused a sudden growth of the shear layer width. Corcos and Lin[17] performed linearized 3-D simulations and reported a hierarchy of motions in which the 2-D roll-up and pairing of spanwise vortices drove the secondary instabilities to produce streamwise vortices in the braid region of the 2-D structures. Three-dimensional effects are further discussed by Metcalfe et al.[18], Lesieur et al.[19], and Rogers and Moser[20].

Davis and Moore[21] studied the manipulation of vortex pairing through the forcing of 2-D axisymmetric and plane spatially-developing shear layers. The authors showed that the vortex pairing events were determined by inlet boundary conditions with the number of pairings equal to the number of subharmonic modes present in the inlet boundary conditions. The vortex dynamics were found to be relatively independent of Reynolds number. Lowery and Reynolds[22] examined the effect of vortex pairing on time-averaged properties by performing highly resolved 2-D and 3-D spatial DNS of the forced mixing layer. The forcing function for the 2-D simulations consisted of the fundamental, and first and second subharmonic modes with no explicit phase shift. Around each region of vortex pairing, the layer experienced rapid growth, and positive turbulence kinetic energy production, while between pairing events, inhibited layer growth and negative turbulent

4

kinetic energy production occurred. The 2-D simulations produced spread rates consistent with those in the 3-D simulations and experiment.

The literature shows that temporal simulations are capable of predicting experimentally observed phenomena such as shear layer rollup, vortex pairing, as well as experimentally measured spread rates. However, the spatial reference frame must be adopted to realize asymmetric entrainment in which a greater proportion of high speed fluid is entrained into the layer, dispersion of instability waves due to mode dependent phase speed as predicted by spatial stability theory, and feedback effects whereby downstream events influence the development of upstream events.

In the present study, effects of Reynolds number and inlet forcing functions are investigated with a 2-D simulation of the spatially evolving mixing layer. Several inlet conditions are considered, based on discrete modes from linear stability theory and based on energy spectra and intensity from experimental observations. Combinations of both discrete and broad band mode forcing are also utilized to investigate the complex interactions which occur in experimental attempts to control shear layer growth through large amplitude forcing of turbulent jets. A unified treatment is presented of which can be used to explain many phenomena which have been observed in several different studies, some apparently in conflict. The need for some forcing of the inlet, and the type required in order to reproduce experimental data are discussed. In addition, two-point spatial and auto-correlations are used to determine the size of the coherent structures.

5

## II. GOVERNING EQUATIONS

The equations of motion governing two-dimensional, incompressible, unsteady fluid flow are:

$$\frac{\partial u_j}{\partial x_j} = 0 \tag{1}$$

$$\frac{\partial u_i}{\partial t} + \frac{\partial}{\partial x_j}(u_i u_j) = -\frac{1}{\rho}\frac{\partial p}{\partial x_i} + \nu\frac{\partial^2 u_i}{\partial x_j \partial x_j} \tag{2}$$

where the unknown variables are $u = u_1$, $v = u_2$, and $p$, which are the $x$- and $y$-component velocities, and pressure, respectively. No spatial filtering of the governing equations is performed because the flow is dominated by the large scales. The assumption of two-dimensionality impedes the formation of small scales via vortex stretching, whereas the smallest scales which may be present in the inlet conditions are dissipated. The coordinate system, flow parameters, and computational domain used in the simulations are shown in Fig. 1.

Simulations were started with initial conditions consisting of the streamwise component of velocity, $u$, set to the same reference hyperbolic tangent profile everywhere in the computational domain, and $v = p = 0$. The domain of interest for the present study starts at some distance downstream of the splitter plate where the high and low speed streams have merged to form a monotonic velocity profile. The hyperbolic tangent profile is adopted in the current study, which defines the mean streamwise velocity component, $U_1$, at the inlet as:

$$U_1(y) = U_C\{1 + \lambda\tanh\left(\frac{2y^*}{\delta_{w_o}}\right)\} \tag{3}$$

where $y^* = y - H/2$, $U_C = \frac{1}{2}(U_H + U_L)$ is the convective velocity, $\lambda = (U_H - U_L)/(U_H + U_L)$ is the velocity ratio, and $\delta_{w_o} = (U_H - U_L)/(\partial u/\partial y)_{o_{max}}$ is the vorticity thickness at the inlet cross section (denoted by subscript "$o$"), with $(\partial u/\partial y)_{o_{max}}$ being the maximum derivative at the inlet cross-sec-

6

tion. The vorticity thickness is a measure of the shear layer width and for this study, $\delta_{\omega_o} = 0.1359$ is used. For the hyperbolic tangent profile, the initial momentum thickness is given by, $\theta_o = \delta_{w_o}/4$. The mean flow at the inlet is approximated as parallel, resulting in a zero mean transverse velocity, $U_2(y) = 0$. The zero-gradient boundary condition is used in all cases for the specification of the instantaneous pressure at the inlet boundary, $\partial p/\partial x_1 = 0$.

Two classes of perturbations are used in the current study: (*i*) perturbations derived from linearized inviscid stability analysis, and *(ii)* perturbations derived from experimentally measured velocity spectra and transverse root mean square (*rms*) values. The inlet boundary condition is then a superposition of the mean and perturbed velocity fields. The two classes of perturbations are defined below.

*(i)* Perturbations from linearized inviscid stability analysis

The first class of perturbations is derived from the solution of the Rayleigh equation governing the instability of the reference hyperbolic tangent profile to spatially developing disturbances. The solution yields the set of complex eigenfunctions corresponding to a specified frequency, $\omega_p$. In this study, various combinations of the fundamental (the mode which inviscid theory predicts the most amplified growth rate), and the first and second subharmonic modes are used as perturbations. In simulations forced with more than one discrete mode, no explicit phase shift was introduced between the modes. A complete derivation and solution of the Rayleigh equation is provided by Monkewitz and Huerre[13], with the general form of the perturbation being:

$$u'_i(y, t) = \text{Real} \{ \tilde{u}_i^p(y) e^{i\omega_p t} \} \tag{4}$$

with $i = \sqrt{-1}$, $t$ being the time, and $\tilde{u}_i^p(y)$ being the complex eigenfunction for the mode with angular frequency, $\omega_p$. The eigenfunctions for the fundamental, first, and second subharmonic modes, were obtained from Lowery and Reynolds[22].

*(ii)* Random perturbations from experimental data

Perturbations having a broad spectrum resembling that of fully-developed, mostly random, 3-D turbulence were generated. The perturbations are typical of those found in the experimental mixing layer originating from turbulent boundary layers upstream of the splitter plate, with the obvious difference that the conditions generated here are 2-D, while those of the experiment are 3-D. The velocity power spectra and root-mean-square *(rms)* perturbation levels were taken from the experiment of Spencer and Jones[23]. Because phase information is not included in the power spectra, a random phase relationship for the modes comprising the spectra was assumed. The velocity components are found by performing a Fourier transform of the complex Fourier coefficients, $a_i(f)$, defined by:

$$a_i(f) = \left[ \frac{F_i(f)\, \overline{u_i'^2}\, T}{4\pi^2} \right] (\cos\gamma + i\sin\gamma) \tag{5}$$

where $f$ is the frequency, $F_i(f)$ is the normalized spectrum function measured experimentally, $\overline{u_i'^2}$ is the *rms* level of the $i^{th}$ velocity component also measured experimentally, $T$ is the time interval to generate boundary conditions (typically four times the total period of simulation desired), and $\gamma$ is the randomly generated phase angle. The complete details of the derivation of time-dependent inlet boundary conditions based on a experimentally measured spectra are given in Wilson[24].

8

The convective boundary condition is applied at the outflow boundary in the current simulations to allow the developing structures to flow smoothly out of the computational domain. Written in terms of the general variable, $\phi$, the convective boundary condition is given by:

$$\frac{\partial \phi}{\partial t} + U_c \frac{\partial \phi}{\partial x_1} = 0 \tag{6}$$

No-stress boundary conditions are applied at the free-streams located at the top and bottom of the computational domain. In addition, the free-stream boundary is placed at a transverse distance such that there are no interactions between the developing structures and the boundaries, which would violate the no-stress condition. The no-stress boundary conditions are approximated as $p =$ constant along the upper and lower boundaries and $\partial u_i / \partial x_2 = 0$.

The cell-centered, finite-volume approach is used to integrate the continuous governing equations, given by equations (1) and (2), over a typical nine-point control volume which yields a discretized system of algebraic equations to be solved simultaneously. Simulations are performed with a third-order upwind biased approximation of convection terms following Leonard[25]. The diffusive flux at the cell-face is approximated using fourth-order central differences. Thus, the formal spatial accuracy of the numerical scheme is third-order. A third-order fully implicit time discretization is applied to the temporal derivative. Hence, iteration is required at each time step. Details of the numerical scheme are presented in Wilson[24]. A typical simulation with a grid of $320 \, x \, 100$ over a domain size of $L \, x \, H = 20 \, x \, 8$, requires approximately 3 1/2 hours of CPU time on a single processor of the Cray C-90 supercomputer.

## III. ACCURACY OF NUMERICAL FORMULATION

The accuracy of the numerical method is checked by comparison of the growth rates of single frequency disturbances with those predicted by inviscid theory. Minimum grid points for accurate resolution of each wave can thus be determined. Given a base velocity profile, linear stability theory can predict the initial growth rates of instability waves. At high Reynolds numbers viscous effects are negligible so that inviscid theory can be used. Monkewitz and Huerre[13] have computed growth rates for a range of $\beta$ (the non-dimensional angular frequency, $\equiv 2\pi f \theta_o / U_C$) using linear inviscid stability theory. They found that modes with $\beta < 0.5$ had exponentially increasing growth rates whereas those with $\beta > 0.5$ experienced exponentially decreasing growth rates. The most amplified mode had $\beta = 0.22$ and this mode was referred to as the fundamental mode. Miksad[26] showed that linear theory is appropriate over the first 1 1/2 wavelengths. Present computations of the growth rates are compared to the results of Monkewitz and Huerre[13] in Fig. 2 for the velocity ratio, $\lambda = 0.5$. For computations in Section IV, the velocity ratio, $\lambda = 0.538$, is utilized. Computations are performed at $Re = 10^4$ for two perturbation frequencies, the fundamental ($\beta = 0.22$) and its subharmonic ($\beta = 0.11$), with the initial forcing strength for both modes being, $(u_{rms}/\Delta u)_{max} = 4.9 \times 10^{-3}$. Three streamwise grid resolutions are utilized. The transverse resolution is chosen to resolve the eigenfunctions of the two modes and is constant for all grids used in this section. The information on the grid distribution and the domain size is summarized in Table 1. Also included is the number of streamwise points per wavelength (*ppw*). For the fundamental mode, the coarse grid has 8 *ppw* and is seen to be inadequate in predicting the growth rate. The intermediate and fine grids have 16 *ppw* and 32 *ppw* respectively and are able to predict the growth rate found from inviscid theory to within roughly 2%. For the subharmonic mode, the coarse (16 *ppw*), intermediate (32 *ppw*), and fine grids (64 *ppw*) predict growth rates which are within roughly 4% of that

10

predicted by linear theory. Therefore, with the present numerical method, at least 16 *ppw* are required to accurately resolve each mode. A comparison of the computed growth rates and those from linear theory is given in Table 2. The simulation at $Re = 10^3$ is essentially the same as those at $Re = 10^4$, whereas at $Re = 10^2$, the predicted growth rates (not shown) are about 20% lower.

**Table 1: Domain sizes for spatial growth rate computations.**

| Mode | Coarse, *ni x nj, ppw* | Intermediate, *ni x nj, ppw* | Fine, *ni x nj, ppw* | *L x H* |
|---|---|---|---|---|
| first subharmonic | 48 x 80, 16 | 96 x 80, 32 | 192 x 80, 64 | 5.84 x 4 |
| fundamental | 24 x 80, 8 | 48 x 80, 16 | 96 x 80, 32 | 2.92 x 4 |

**Table 2: Comparison of growth rates from simulation to linear theory, $Re = 10^4$**

| Mode | Coarse | Intermediate | Fine | Linear theory |
|---|---|---|---|---|
| first subharmonic | 0.071 | 0.071 | 0.071 | 0.074 |
| fundamental | 0.085 | 0.096 | 0.096 | 0.098 |

## IV. RESULTS AND DISCUSSION

The simulations forced with discrete modes can be viewed as unsteady, laminar calculations of instability modes, while those which use a broad-band spectrum as forcing functions, can be viewed as a 2-D approximation of the 3-D turbulent mixing layer observed experimentally[23]. Fig. 3 compares the spectrum from a 3-D experiment to those predicted in the present simulations using (*i*) the fundamental mode and (*ii*) a broad-band of modes. The 3-D experimental spectrum shows a much more gradual decay of the amount of energy in the high frequency range than obtained in our simulation with broad mode forcing. In the latter, the energy is concentrated in a broad band of modes, the highest frequency modes having been removed by dissipation, but the 2-D approximation prevents replenishment via the vortex stretching mechanism. Results of simu-

11

lations forced with a single discrete mode show a concentration of energy at that associated frequency, as expected.

The resulting vortex dynamics for mixing layer simulations using the two sets of perturbations at the inlet boundary are presented in this section. The effect of the vortex dynamics on time-averaged properties are discussed in the next section. Effects of inlet forcing and Reynolds numbers are explored.

When no forcing is applied at the inlet boundary (i.e. steady inlet boundary conditions), time traces of velocity and pressure confirm that little unsteady motion occurs after initial transients have been convected out of the computational domain. The maximum normalized fluctuating velocity within the computational domain was found to be $(u_{rms}/\Delta u)_{max} = 0.001$, where $u_{rms}$ is the *rms* of the streamwise fluctuating velocity and $\Delta u = U_H - U_L$. If some form of forcing is used at the inlet boundary for the period, $0 < t < \tau$, after which the forcing is suspended for, $t > \tau$, the unsteady motion due to the initial forcing is convected out of the computational domain and steady flow results. This finding is in agreement with the spatial simulations of Lowery and Reynolds[21] in that unsteady motion would develop from steady inlet conditions only for extremely long computational domains and/or very large Reynolds numbers. However, such steady inlet conditions are impossible to achieve in physical experiments. Some form of forcing is needed to initiate the instabilities of the mixing layer at moderate Reynolds numbers and realistic computational lengths.

## Vortex Dynamics

### Forcing with Modes from Inviscid Stability Theory

In this section, inlet boundary perturbations are derived from the inviscid stability analysis of Monkewitz and Huerre[13]. Some aspects of discrete mode simulations were discussed in the previous section where single mode simulations were utilized to test the grid resolution requirements of the numerical formulation. A more detailed picture of these simulations is given in this section as well as the results from two and three mode simulations.

The time, $t$, is non-dimensionalized by the eddy flow-through time, $\tau_e = L/U_C$, which is the time required for a structure to travel from the inflow to the outflow at the convective velocity. The vorticity contours at $t = 2.708$ seconds, for a simulation forced by the fundamental mode, are shown in Fig. 4 for a computational domain of $L \, x \, H = 12 \, x \, 4$ with $ni \, x \, nj = 200 \, x \, 100$ grid points. This simulation shows that the initially uniform vortex sheet at $t = 0$, "rolls up" into intense "lumps" of spanwise vorticity separated by a distance of the fundamental wavelength ($\lambda = 0.985$). This process is the so-called primary or Kelvin-Helmholtz instability. After a distance of roughly 2 1/2 wavelengths ($x = 2.5$) from the inflow, the roll-up of the shear layer saturates and experiences a decay for the remaining spatial extent.

Many experimental and numerical studies have shown that in the absence of subharmonic frequencies, vortex pairing does not occur. To test the effects of dual-mode forcing, simulations were carried out with forcing consisting of the fundamental and first subharmonic modes at equal initial amplitudes such that the *rms* of streamwise velocity at the inlet was $(u_{rms}/\Delta u)_{max} = 0.06$. This simulation was carried out using the same computational grid and duration as the fundamental mode simulation previously discussed. Vorticity contours for the two-mode simulation at $t =$

13

2.708 seconds are shown in Fig. 5. After the initial start-up period, regular periodic motion occurs for $t > 1.625$ seconds. The first two fundamental wavelengths $(0 < x < 2)$ are similar to the single mode simulation, while downstream the flow is drastically different. At $x = 4$, the subharmonic mode is of sufficient strength to vertically displace the lumps of vorticity separated by fundamental wavelengths. This causes the two neighboring vortices to rotate about their common center and coalesce forming a new larger structure which results in a rapid growth of mixing layer width at the location of vortex pairing. Downstream of the pairing location, the new structure rotates clockwise through a small angle and is convected out of the domain with the spacing between the new structures being one subharmonic wavelength $(\Lambda = 1.97)$.

A three-mode simulation was carried out using the fundamental, first, and second subharmonic modes from inviscid theory as inlet forcing functions such that $(u_{rms}/\Delta u)_{max} = 0.05$. The computational length and height of the domain were increased to $L x H = 20 x 8$, with $ni x nj = 320 x 100$ grid points. An expanding grid was used in the transverse direction to enable the rapid changes in the fundamental mode eigenfunctions near the center of the mixing region to be resolved efficiently. One period of the second subharmonic mode is shown in Fig. 6, in which only a section of the computational height $(2 < y < 6)$ is displayed. Note, that the structures move with the convective speed of the flow, $U_C = 0.65$, therefore the structures advance approximately 1.3 units in the downstream direction in the plotting interval (0.065 seconds) shown in Fig. 6. The addition of the second subharmonic mode allows a second vortex pairing to occur at $x = 10$. The time trace and power spectra results (not shown) reveal the transfer of energy from the fundamental to the first subharmonic mode (the first vortex pairing) and then from the first to the second subharmonic mode (the second vortex pairing) as the structures convect from inflow to outflow.

14

## Forcing with a Broad Spectrum of Modes from Experimental Data

The second class of perturbations used as forcing functions is that of a broad spectrum of modes derived from experimentally measured power spectra. This class of inlet boundary conditions is used to simulate the broad range of scales found in fully three-dimensional turbulent flows. Of particular interest is the pairing mechanism and shear layer growth rates compared to one-, two-, and three-mode simulations.

Many computational and experimental mixing layer studies have shown that small scale motions have their origins in the braid region of the two-dimensional structures where streamwise vorticity first appears. Obviously, 2-D simulations are not capable of capturing the energy cascade to small scales and can only simulate the generation, growth, and interaction of the 2-D spanwise vortex structures. The current simulations confirm that for 2-D simulations, small scale motions are not continuously generated. Moreover, if small scale motions are injected at the inlet boundary, they experience rapid decay in agreement with linear theory as discussed previously.

It has been shown, using discrete mode simulations, that periodic forcing with no explicit phase shift between the modes produces complete vortex pairing at fixed spatial locations. The non-periodic inlet boundary forcing used with the broad mode simulations does not produce vortex pairing at fixed spatial locations and pairing occurs somewhat randomly over a region. Vortex tearing, whereby a weaker vortex is pulled apart by its stronger neighboring vortices, can be seen (not shown) in selected vorticity contours of broad mode simulations, due mainly to the presence of finite phase shifts between the various modes in the inlet forcing functions. The effect of the strength of the forcing is compared in Fig. 7a - 7c, which shows vorticity contours at $t = 3.413$ seconds and $Re = 10^2$ for forcing levels of $(u_{rms}/\Delta u)_{max} = 0.0015, 0.015, 0.15$, respectively. The

simulations were carried out with the same computational domain and grid as was used in the three mode simulation. With the full strength forcing amplitude reduced by a factor of 100, Fig. 7a, shear layer roll-up occurs at $x = 10$, but there is no evidence of pairing within the computational domain, $0 < x < 20$. With the forcing amplitude reduced by a factor of 10, Fig. 7b, shear layer roll-up occurs at around $x = 6$, with the first pairing around $x = 14$. The strongly forced case, Fig. 7c, shows that shear layer roll-up occurs immediately downstream of the inlet boundary and the first pairing occurs at around $x = 4.5$. These trends are repeated in Fig. 8, for simulations at $Re$ $= 10^4$. The effect of forcing strength on time-averaged turbulent statistics is discussed in a later section.

Clearly, the effect of inlet forcing is to promote rapid growth of instabilities to amplitudes which are sufficiently high for shear layer roll-ups to occur, and in the presence of sub-harmonics vortex-pairings would take place subsequently. The far-field vortex dynamics are mostly independent of the inlet forcing. The fluctuating intensity of 0.15% corresponding to the forcing levels in Figures 7a and 8a is of the order of the background turbulence in many wind tunnels. In fact, a simulation with no forcing, i.e., completely steady inlet conditions deviates more from practical experimental conditions than one with small forcing. One may speculate that given sufficient length, in the former case, minute instabilities in the form of round-off errors in the computer would ultimately grow sufficiently to produce the same vortex dynamics. Needless to say, there has been no simulation of sufficient length to test this hypothesis.

To confirm that the observed vortex dynamics would continue downstream a simulation was carried out for an expanded domain size of $L \times H = 40 \times 16$ with $ni \times nj = 640 \times 130$ grid points. Figures 7d and 8d show the resulting vorticity contours at $t = 1.625$ seconds for $Re = 10^2$ and $10^4$,

respectively, using the broad mode forcing with the amplitude $(u_{rms}/\Delta u)_{max} = 0.015$. The results at this time step, as well as others not shown, show that the mixing layer continues to grow through vortex pairing for the additional length, $20 < x < 40$. The time trace results at various points along the length of the layer centerline show that the dominant frequency shifts from $f = 0.8$ at $x = 3$ to $f = 0.08$ at $x = 36$. It is apparent that on the average, approximately four pairings have taken place because the dominant frequency has been halved four times.

### Forcing with Mixed Modes

To approximate experiments in which the shear layer is forced with a few discrete modes, two additional simulations at $Re = 10^4$ are discussed in this section. The first simulation, which will be referred to as case b, uses the fundamental mode with strength, $(u_{rms}/\Delta u)_{max} = 0.015$, superimposed on the broad mode forcing function used in the weakly forced simulation (Fig 8a, referred to as case a), which had a strength, $(u_{rms}/\Delta u)_{max} = 0.0015$. The second simulation, referred to as case c, uses the fundamental and the first subharmonic modes of equal strength, $(u_{rms}/\Delta u)_{max} = 0.0015$, along with the weak broad modes used in case b. Vorticity contours at $t = 3.413$, are compared in Figures 9a - 9c for cases a - c, respectively. The addition of the fundamental mode which is one order of magnitude larger than the broad mode forcing function (Fig 9b) results in shear layer roll-up at an earlier streamwise location of $x = 2$. However, the location of the initial vortex pairing is shifted downstream from $x = 8.5$ (Fig 9a) to $x = 9.5$ (Fig 9b). The addition of the fundamental and first subharmonic modes (Fig 9c) results in shear layer roll-up and a large shift in the location of the first vortex pairing, from $x = 8.5$ (Fig 9a) to $x = 4$ (Fig 9c), but with no vortex interaction in the region, $5 < x < 13$. Time trace results (not shown) indicate that the second subharmonic mode which is present in the weak broad mode forcing increases gradually in this region,

17

but does not grow to sufficient strength to produce a second pairing within the computational domain, unlike in the simulations of cases a and b. It appears that the addition of the first subharmonic mode in case c suppresses the growth of the second subharmonic mode[16] thereby resulting in a large region with no vortex interaction and stagnation of mixing layer growth. The momentum thickness of the shear layer is defined by the following integral:

$$\theta = \frac{1}{H} \int_0^H (u_H - u)(u - u_L) \, dy \qquad (7)$$

Time-averaged momentum thicknesses for the three cases are shown in Fig 9d. It can be seen that the addition of the fundamental mode in case b, results in a slight increase in layer width in the region, $2 < x < 4$, followed by a slight decrease in the region, $5 < x < 10$. The addition of the fundamental and first subharmonic modes in case c, results in a significant increase in shear layer width in the region, $1 < x < 6$, followed essentially by no growth in the region, $6 < x < 14$. Shear layer growth is resumed for $x > 14$ with the growth of the second subharmonic mode. From the previous discussion, the role of the low amplitude broad mode forcing is to provide a supply of subharmonics to produce vortex pairing after the discretely forced modes have saturated. This is apparent by comparing the simulation shown in Fig 4 (fundamental mode only) to that shown in Fig 9b (fundamental mode and weak broad mode forcing).

Three-dimensional, temporal simulations utilizing a discrete mode superimposed on a broad spectrum of modes were performed by Riley and Metcalfe[14]. Their results show that the addition of the fundamental mode to strong background turbulence (of 18% intensity), which is similar in spectrum to the broad band forcing used in this paper, resulted in an increased initial growth of the shear layer, followed by a suppressed growth rate in comparison to results using only background turbulence. Those trends are in agreement with the results of case a and b. The experimental study

18

of forced mixing layers by Oster and Wygananski[27] utilized a single frequency disturbance to force the shear layer. Their results showed that the unforced mixing layer (with only a small level of background turbulence of roughly 0.2% intensity) exhibited constant linear growth, while the addition of the discrete mode showed increased growth rates in the near field, followed by regions of zero growth in which it was shown that no vortex interaction took place, followed by resumed mixing layer growth. The present results are in complete agreement with those experimental observations.

## Effect of Reynolds Number

The effect of Reynolds number for a single mode simulation has already been discussed. It was shown that the medium to high Reynolds number simulations ($Re > 10^3$) yield close agreement with spatial growth rates predicted by linear inviscid theory. For low Reynolds number simulations, $Re_{\delta_o} = 100$, the spatial growth rates are mildly damped compared to linear inviscid theory and there is a mild smearing of the rolled-up structures. Davis and Moore[21] report similar trends in their one-, two-, and three-mode simulations, with reduced Reynolds number simulations affecting only the sharpness of the vortical structures. The authors report that the vortex dynamics are not changed by reducing the Reynolds number from $10^4$ to 25. These results support the claim that for two-dimensional simulations involving only a few discrete modes from linear stability theory as forcing functions, the Reynolds number is of minor importance in computing the vortex dynamics of the shear layer.

The broad spectrum forcing function contains many high frequency modes which are more susceptible to viscous forces than their low frequency counterparts. Simulations using the broad

19

spectrum forcing function were carried out at $Re = 10^4$ to determine if the decreased damping of high frequency modes would result in a change in the pairing mechanism discussed previously.

An inspection of the vorticity contours in Fig. 8 for the $Re = 10^4$ simulations reveals that the shear layer rolls up and pairs much earlier in comparison to the $Re = 10^2$ simulations. Also, the vortices tend to maintain their individual identities after pairing while the increased viscous forces of the $Re = 10^2$ simulations, tend to smear out the individual vortices and create a more uniform core for the paired structures.

The effect of the strength of forcing is compared in Fig. 8 for the $Re = 10^4$ simulations. The forcing levels in Figures 8a - c are $(u_{rms}/\Delta u)_{max}$ = 0.0015, 0.015, and 0.15, respectively, with identical inlet boundary conditions and grid used for the $Re = 10^2$ simulation shown in Fig. 7. With the smallest forcing amplitude, Fig. 8a, the shear layer rolls up at around $x = 5$ and the first pairing occurs at around $x = 9$. Recall that the same forcing level produced no vortex pairing for the $Re = 10^2$ simulation. With the intermediate forcing amplitude, Fig. 8b, shear layer roll-up occurs at about $x = 3$, with the first pairing at around $x = 6$. The full strength forcing results, shown in Fig. 8c show that the layer rolls up very close to the inflow boundary and the first pairing occurs around $x = 3$. This confirms the conclusions reached using single mode simulations, in that decreasing the Reynolds number has a damping effect on the growth rate of disturbances. The simulations at $Re = 10^4$ suggest that the streamwise location of the initial vortex pairing scales linearly with the log of the inlet forcing amplitude, which is not surprising since linear theory predicts exponential growth rates for these instability waves.

## Time-Averaged Properties

This section discusses the time-averaged properties of the mixing layer. In particular, the effect of the inlet boundary conditions and coherent structures on mixing layer growth, time-averaged velocity profiles, and turbulence statistics are investigated.

### Discrete-Mode Forcing

Three normalized shear layer widths are calculated with the first based on the transverse distance between locations where the property $\phi = 0.9$ and $\phi = 0.1$, with $\phi = (u - u_L) / (u_H - u_L)$. The second normalized width is the momentum thickness which was defined previously The third width is the normalized vorticity thickness, $\delta_\omega$, which was defined previously in Section II. The vorticity thickness shows more drastic changes in shear layer width because it is a differential quantity, while the momentum thickness is an integral quantity and is thus smoother.

Figures 10 and 11 show time-averaged results for the three mode simulation averaged over three periods of the second subharmonic mode. The shear layer widths displayed in Fig. 10a clearly show the effect of the two spatially fixed vortex-pairing events which occur roughly at $x = 4$ and $x = 10$. The shear layer width experiences a drastic reduction after the second vortex pairing around the region $x = 13.5$, after which the layer growth is arrested. The cause of the decrease in layer width can be determined by examining the vorticity contours shown in Fig. 6. The second vortex pairing occurs at $x = 10$ where the two vortices are aligned vertically and reach maximum transverse separation. Downstream of this point, the elongated structure rotates clockwise and achieves a horizontal orientation at roughly $x = 13.5$ (seen at $t = 1.755$ seconds, Fig. 6c). Still further downstream, the structure thickens in the transverse direction slightly as it convects through the outflow boundary. The horizontal orientation of the elongated structure at $x = 13.5$ results in a

21

decrease in mixing layer width along with negative Reynolds shear stress. The resulting negative Reynolds shear stress can be deduced from the orientation of the vortex pairing as noted by Ho and Huerre[27]. Before the two vortices pair and reach their vertical orientation (Fig. 6c, $x = 9.5$), the correlation of vertical and horizontal velocity fluctuations produces positive Reynolds stresses, while after they reach their vertical orientation (Fig. 6d, $x = 11$), negative Reynolds shear stress results.

Fig. 10b displays the time-averaged $u$ component profiles which show self-similarity except at cross sections where pairings occur ($x = 4$ and $x = 10$). The $v$ component profiles, after the second pairing at $x = 12.4$, shown in Fig. 10c, reveal negative mean transverse velocity at the bottom of the computational domain which results in transport of fluid away from the mixing layer. Fig. 11a shows characteristic double "hump" $u_{rms}$ profiles for cross sections after the second pairing ($x > 12$) and Fig. 11c shows relatively large negative Reynolds shear stress for the region of decreasing layer width ($x = 12.4$) as explained above. The turbulence statistics are compared to experimental data from the forced shear layer experiments of Oster and Wygnanski[27]. The double hump $u_{rms}$ profile is also apparent in this experiment, although it is not as pronounced as in the current 2-D simulations.

## Broad-Spectrum-Mode Forcing

Recall that forcing with periodic inlet boundary conditions from inviscid theory produces vortex pairing at fixed spatial locations, while quasi-random broad spectrum forcing produces vortex pairings which are distributed over a range of spatial locations. As a result, the time-averaged vorticity, pressure, and shear layer widths vary more smoothly than the time-averaged properties from the three mode simulation. The broad mode simulations at $Re = 10^2$ and $Re = 10^4$, Figures

7d and 8d, respectively, are used to calculate spread rates, mean velocity profiles, and turbulence statistics over the interval, $1.056 < t < 4.063$ seconds which represents roughly 3 eddy flow-through times. From analysis of time trace results of the $Re = 10^2$ simulation, roughly 120 structures have been generated just downstream of the inflow and about 20 structures have passed through the outflow in this time interval. The time-averaged results for these simulations are presented in Fig. 12 and 13. In comparison to the 3-mode simulation (Fig. 10a), the continuous supply of subharmonics in this case results in continued linear growth of the shear layer. Mean streamwise velocity profiles show self-similarity throughout the domain, while mean transverse velocity profiles show that on the average fluid is entrained into the mixing region. Profiles of streamwise fluctuating velocities (Fig. 13a) show that the double hump profiles found in the 3-mode simulations are absent. The results are in reasonable agreement with experimental observations for unforced shear layers. Reynolds shear stress profiles (Fig. 13c) are positive and similar in magnitude to those measured in the vortex interaction region of Oster and Wygnanski[27]. The magnitude of the transverse fluctuating velocity is overpredicted by approximately 40% in the current 2-D simulations. Lowery and Reynolds[22] made similar observations in their 2-D simulations while their 3-D simulations yielded the experimentally measured magnitude. The discrepancy is clearly due to the absence of energy transfer to small scales due to vortex stretching. The same general trends are observed at both Reynolds numbers, except that the profiles vary more sharply at the higher Reynolds number. Spread rates computed from the discrete and broad spectrum simulations are presented and compared to experimental values in Table 3 in the following normalized form:

$$\frac{1}{\Delta u}\frac{d\theta}{dt} = 2\lambda\frac{d\theta}{dx} \qquad (8)$$

It can be seen that the spread rate in the three-mode simulation is greatly enhanced in the region prior to the second vortex pairing event $(150 < x/\theta < 240)$. Also, the broad spectrum simulations at $Re = 10^2$ and $10^4$ yield nearly identical spread rates in the far-field which are similar to the far-field spread rates measured experimentally.

**Table 3: Comparison of computed spread rates with experimental values.**

| Study | $Re$ | Region | Spread Rate, $\frac{1}{\Delta u}\frac{d\theta}{dt}$ |
|---|---|---|---|
| Current, 3-mode, (Fig. 10a) | $10^2$ | $0 < x/\theta < 120$<br>$130 < x/\theta < 140$<br>$150 < x/\theta < 240$<br>$350 < x/\theta < 600$ | 0.020<br>0.001<br>0.029<br>0.001 |
| Current, broad spectrum, (Fig. 12a) | $10^2$ | $150 < x/\theta < 1000$ | 0.022 |
| Current, broad spectrum, (Fig. 12d) | $10^4$ | $150 < x/\theta < 1000$ | 0.021 |
| Wygnanski & Fieldler[29] | $10^5$ | - | 0.022 |
| Spencer and Jones[23] | $10^6$ | - | 0.016 |
| Oster and Wygnanski[27] | $10^4$ | $0 < x/\theta < 400$<br>$400 < x/\theta < 600$<br>$600 < x/\theta < 1500$ | 0.030<br>0.003<br>0.022 |

The effect of the forcing strength on the streamwise development of the maximum cross-sectional value of $u_{rms}$ and $v_{rms}$ is presented in Figures 14 and 15. The results at $Re = 10^2$ are not completely independent of forcing level, while the $Re = 10^4$ far-field results ($x > 10$) show only minor sensitivity to initial forcing level. One comes to the conclusion that the larger growth rate with increased Reynolds number results in asymptotic values at earlier streamwise locations. The computational length, $L = 20$, would need to be increased to achieve similar forcing insensitivity in the $Re = 10^2$ simulation. Fig. 15 directly compares the $Re = 10^2$ and $10^4$ simulations for the

intermediate forcing level and increased length, $L = 40$. With the length doubled, the turbulent statistics from the $Re = 10^2$ simulation slowly approach those of the $Re = 10^4$ simulation in the far-field. The $u_{rms}$ values appear to approach the asymptotic values more slowly than the $v_{rms}$ values.

**Estimation of Length and Time Scales**

Two-point spatial correlations and autocorrelations were computed at locations along the centerline of the mixing layer to estimate the size and lifetime of the coherent structures. The turbulent statistics of the plane mixing layer are not isotropic, therefore streamwise and transverse correlations are considered separately. It has been shown that the coherent structures move downstream at the convective velocity. Davies et al.[30] used this information and showed that an envelope of maximum correlation can be formed by computing the autocorrelation in a moving reference frame which travels with the convective velocity along the mixing layer centerline. The autocorrelation is then given by:

$$R_{ij}(x_o, y_o, \tau) = \frac{\overline{u'_i(x_o, y_o, t) u'_j(x_o + U_C\tau, y_o, t + \tau)}}{\left[\overline{u'_i(x_o, y_o, t)^2} \, \overline{u'_j(x_o + U_C\tau, y_o, t + \tau)^2}\right]^{1/2}} \qquad (9)$$

where $x_o, y_o$ is the location where the correlation is computed ($y_o$ is located transversely on the layer centerline with $\phi = 0.5$), and $\tau$ is the temporal separation normalized by $\Delta u$ and $\delta_{wo}$. Thus, the reference frame moves a distance of $r = U_C\tau$ along the layer centerline in the time, $\tau$. The autocorrelation was used to estimate the lifetime of the coherent structures at various streamwise locations.

The $R_{11}$ and $R_{22}$ autocorrelations at 4 streamwise locations are shown in Fig. 16. The results show that the structures at the first location (Fig. 16a and 16e) have short lifetimes and become decorrelated in a relatively short period of time compared to later spatial locations. Thus, the iden-

25

tities are lost through the vortex-pairing mechanisms, whose wavelengths increase downstream. The intersection of a parabola, fit to the data at $\tau = 0$, and the horizontal axis gives an estimate of the micro time scale or lifetime of the coherent structures. These results do not confirm the presence of a feedback mechanism suggested by Dimotakis and Brown[3] which would ensure that the structures are correlated all the way upstream to the inlet plane. The integral time scales for the $Re = 10^2$ simulation are roughly 50% larger than those for the $Re = 10^4$ simulation. The larger growth rate of disturbances at $Re = 10^4$ results in a faster turnover time with the structures becoming decorrelated at earlier times.

The transverse size of the coherent structures was estimated using two-point spatial correlations which requires prescribing the spatial separation, $r$, along the transverse direction with zero time separation. The two-point correlation is given by:

$$R_{ij}(x_o, y_o, r) = \frac{\overline{u'_i(x_o, y_o, t)\, u'_j(x_o, y_o + r, t)}}{\left[\overline{u'_i(x_o, y_o, t)^2}\ \overline{u'_j(x_o, y_o + r, t)^2}\right]^{1/2}} \tag{10}$$

The $R_{22}$ spatial correlations are shown in Fig. 17. As expected the transverse size of the structures increase from inflow to outflow, with similar trends for both Reynolds number simulations.

## V. CONCLUSION

Numerical simulations of the spatially-developing two-dimensional mixing layer have been performed with a variety of unsteady perturbations of the inlet boundary conditions used as forcing functions. The forcing functions are used to trigger the instabilities which occur naturally in mixing layer flows. Moreover, these instabilities can be exploited to alter drastically the time-averaged properties of the flow.

Two types of perturbations were considered; *(i)* one-, two-, and three-mode combinations of eigenfunctions corresponding to the solution of the inviscid stability equations and; *(ii)* random inlet boundary conditions derived from experimentally measured power spectra. The simulations using a single mode from inviscid theory show that over the first wavelength the perturbations experience exponential growth resulting in shear layer roll-up, followed by saturation and eventual decay. The presence of subharmonic modes in the inlet boundary conditions produced vortex pairing, with the number of such pairing events equal to the number of subharmonics present in the inlet boundary conditions. Saturation occurred once the supply of subharmonics were exhausted followed by decay. Thus, enhanced mixing due to discrete mode forcing occurs only over limited distances. For simulations forced with a broad spectrum of modes derived from experiment, vortex pairing occurred over a region but not at fixed locations as with the discrete-mode simulations. Three vortex mergings at one spatial location could be observed in the broad spectrum simulations as well as the process of vortex shredding.

The Reynolds number was shown to greatly affect the locations of the initial shear layer roll-up in the broad mode simulations. For low Reynolds number simulations, the additional viscous forces damp the development of shear layer roll-up resulting in delayed roll-up and vortex pairing. With increased Reynolds number, the shear layer roll up is triggered at a shorter streamwise location resulting in a near field which spreads more rapidly than the layer in the low Reynolds number simulation.

It was shown that the streamwise location of the initial vortex pairing scales linearly with the log of the amplitude of the inlet boundary conditions. Vortex pairing was shown to be the dominant mechanism for shear layer growth even up to $1000\theta_o$. The effect of forcing functions on

27

time-averaged flow properties such as mean velocity, shear layer spread rate, and turbulence statistics were investigated. The present two-dimensional simulations captured many experimentally observed phenomena. Computed spread rates agreed very well with those from experimental measurements. Time-averaged properties also displayed similar features observed experimentally.

## ACKNOWLEDGEMENTS

28

# REFERENCES

[1] G. Brown and A. Roshko, "On Density Effects and Large Structure in Turbulent Mixing Layers," J. Fluid Mech. 64(4), 775 (1974).

[2] C. D. Winant and F. K. Browand, "Vortex Pairing: The Mechanism of Turbulent Mixing-layer Growth at Moderate Reynolds Number," J. Fluid Mech. 63(2), 237 (1974).

[3] P. E. Dimotakis and G. L. Brown, "The Mixing Layer at High Reynolds Number: Large-structure Dynamics and Entrainment," J. Fluid Mech. 78(3), 535 (1976).

[4] C-M. Ho and L-S. Huang, "Subharmonics and Vortex Merging in Mixing Layers," J. Fluid Mech. 119, 443 (1982).

[5] C-M. Ho, Y. Zohar, J. K. Foss, and J. C. Buell, "Phase Decorrelation of Coherent Structures in a Free Shear Layer," J. Fluid Mech. 230, 319 (1991).

[6] C. Chandrsuda, R. D. Mehta, A. D. Weir, and P. Bradshaw, "Effect of Free-Stream Turbulence on Large Structure in Turbulent Mixing Layers," J. Fluid Mech. 85(4), 693 (1978).

[7] F. K. Browand and B. O. Latigo, "Growth of the Two-Dimensional Mixing Layer from a Turbulent and Nonturbulent Boundary Layer," Phys. Fluids 22, 1011 (1979).

[8] A. K. M. F. Hussain and K. B. M. Q. Zaman, "An Experimental Study of Organized Motions in the Turbulent Plane Mixing Layer," J. Fluid Mech. 159, 85 (1985).

[9] S. F. Birch, "The Effect of Initial Conditions on High Reynolds Number Jets," AIAA Paper 83-1681 (1983).

[10] P. Bradshaw, "The Effect of Initial Conditions on the Development of a Free Shear Layer," J Fluid Mech. 26(2), 225 (1966).

[11] A. Michalke, "On the Inviscid Instability of the Hyperbolic Tangent Velocity Profile," J. Fluid Mech. 19, 543 (1964).

[12] A. Michalke, "On Spatially Growing Disturbances in an Inviscid Shear Layer," J. Fluid Mech. 23(3), 521 (1965).

[13] P. A. Monkewitz and P. Huerre, "Influence of the Velocity Radio on the Spatial Instability of Mixing Layers," Phys. Fluids 25(7), 1137 (1982).

[14] J. J. Riley and R. W. Metcalfe, "Direct Numerical Simulation of a Perturbed, Turbulent Mixing Layer," AIAA Paper 80-0274.

[15] A. B. Cain, W. C. Reynolds, and J. H. Ferziger, "A Three-Dimensional Simulation and Early Turbulence in a Time- Developing Mixing Layer," Report TF-14, Mech. Engr. Dept., Stanford Univ. (1981).

[16] G. M. Corcos and F. S. Sherman, "The Mixing Layer: Deterministic Models of a Turbulent Flow. Part 1. Introduction and the Two-Dimensional Flow," J. Fluid Mech. 139, 29 (1984).

[17]G. M. Corcos and S. J. Lin, "The Mixing Layer: Deterministic Models of a Turbulent Flow. Part 2. The Origin of the Three-Dimensional Motion," J. Fluid Mech. **139**, 67 (1984).

[18]R. W. Metcalfe, S. A. Orszag, M. E. Brachet, S. Menon, and J. J. Riley, "Secondary Instability of a Temporally Growing Mixing Layer," J. Fluid Mech. **184**, 207 (1987).

[19]M. Lesieur, C. Staquet, P. Le Roy, and P. Comte, "The Mixing Layer and its Coherence Examined from the Point of View of Two-Dimensional Turbulence," J Fluid Mech. **192**, 511 (1988).

[20]M. M. Rogers and R. D. Moser, "The Three-Dimensional Evolution of a Plane Mixing Layer: the Kelvin-Helmholtz Rollup," J. Fluid Mech. **243**, 183 (1992).

[21]R. W. Davis and E. F. Moore, "A Numerical Study of Vortex Merging in Mixing Layers," Phys. Fluids **28(6)**, 1626 (1985).

[22]P. S. Lowery and W. C. Reynolds, "Numerical Simulation of a Spatially-Developing, Forced, Plane Mixing Layer," Report TF-26, Mech. Eng. Dept., Stanford Univ. (1986).

[23]B. W. Spencer and B. G. Jones, "Statistical Investigations of Pressure and Velocity Fields in the Turbulent Two-Stream Mixing Layer," AIAA Paper 71-613 (1971).

[24]R. V. Wilson, "Numerical Simulations of Two-Dimensional, Spatially-Developing Mixing Layers," Masters Thesis, Old Dominion University (1993).

[25]B. P. Leonard, "A Stable and Accurate Convection Modelling Procedure Based on Quadratic Upstream Interpolation," Comput. Methods Appl. Mech. Eng. **19**, 59 (1979).

[26]R. W. Miksad, "Experiments on the Nonlinear Stages of Free-Shear-Layer Transition," J. Fluid Mech. **56(4)**, 695 (1972).

[27]D. Oster and I. Wygnanski, "The Forced Mixing Layer Between Parallel Streams," J. Fluid Mech. **123**, 91 (1982).

[28]C-M. Ho and P. Huerre, "Perturbed Free Shear Layer," Ann. Rev. Fluid Mech. **16**, 365 (1984).

[29]I. Wygnanski and H. E. Fieldler, "The Two-Dimensional Mixing Region," J. Fluid Mech. **41(2)**, 327 (1970).

[30]P. O. A. L. Davies, M. J. Fisher, and M. J. Barratt, "The Characteristics of the Turbulence in the Mixing Region of a Round Jet," J. Fluid Mech. **15(3)**, 337 (1963).
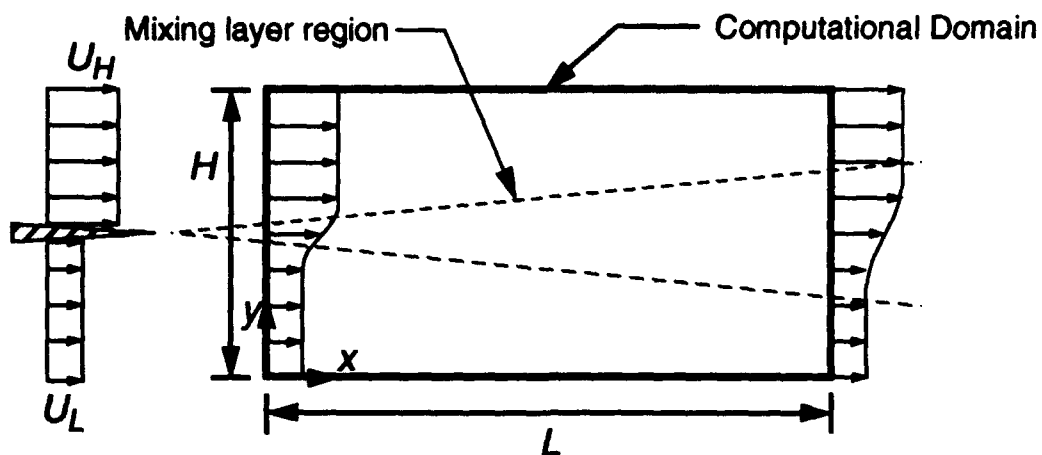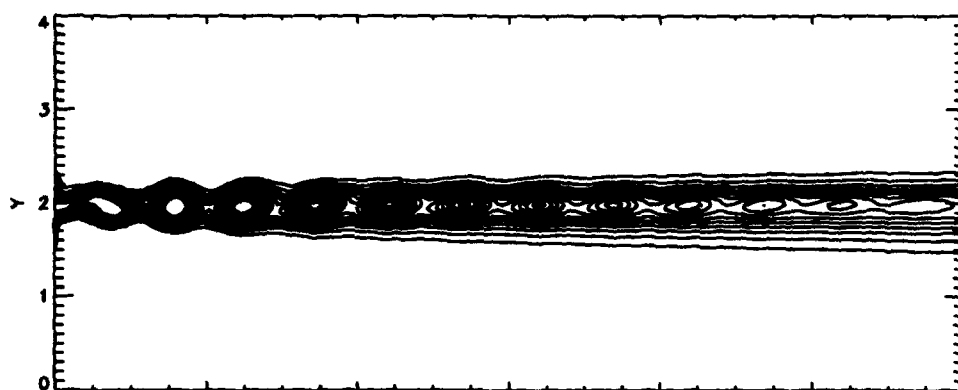
**FIG. 1.** Coordinate system and computational domain for the spatially-developing mixing layer.
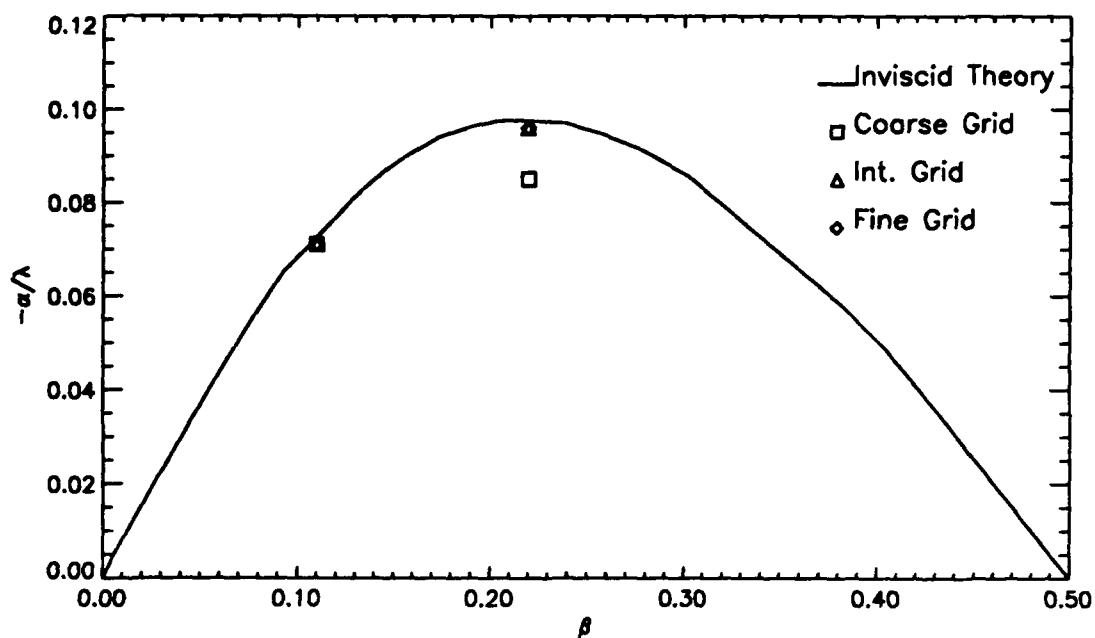


**FIG. 2.** Spatial growth rates from single mode simulations, $\lambda = 0.5$, $Re = 10^4$.
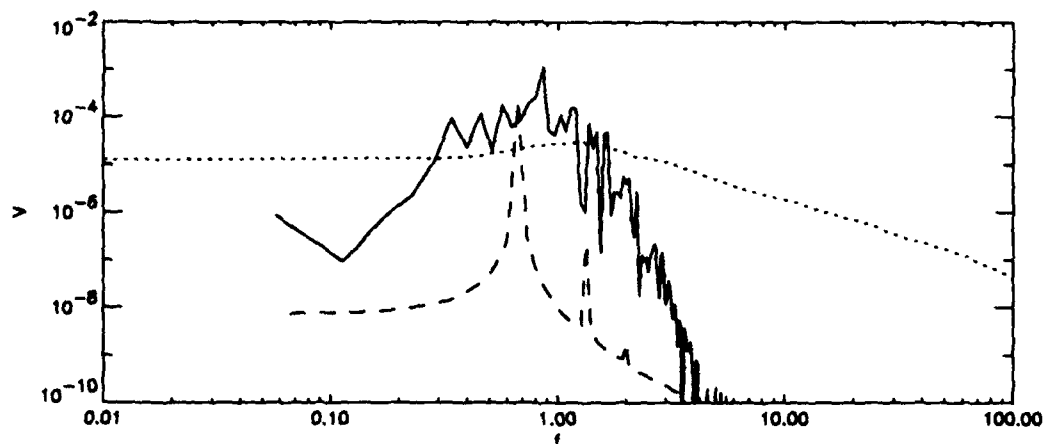
**FIG. 3.** Comparison of v - velocity spectrum of 3-D experiment[23] : ........, with that of present simulations using; broad mode forcing : ———, and discrete (fundamental) mode forcing : - — — -.
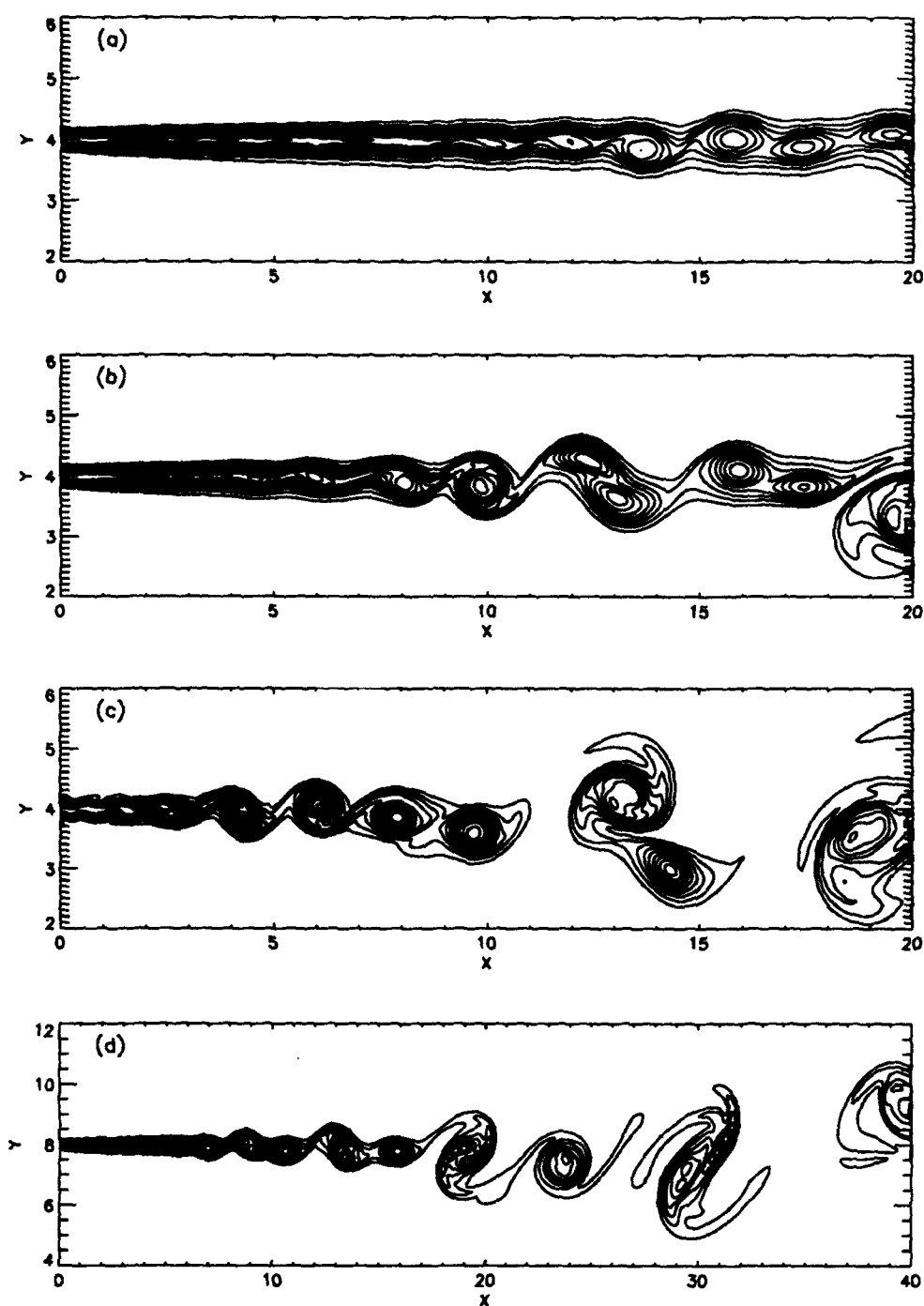


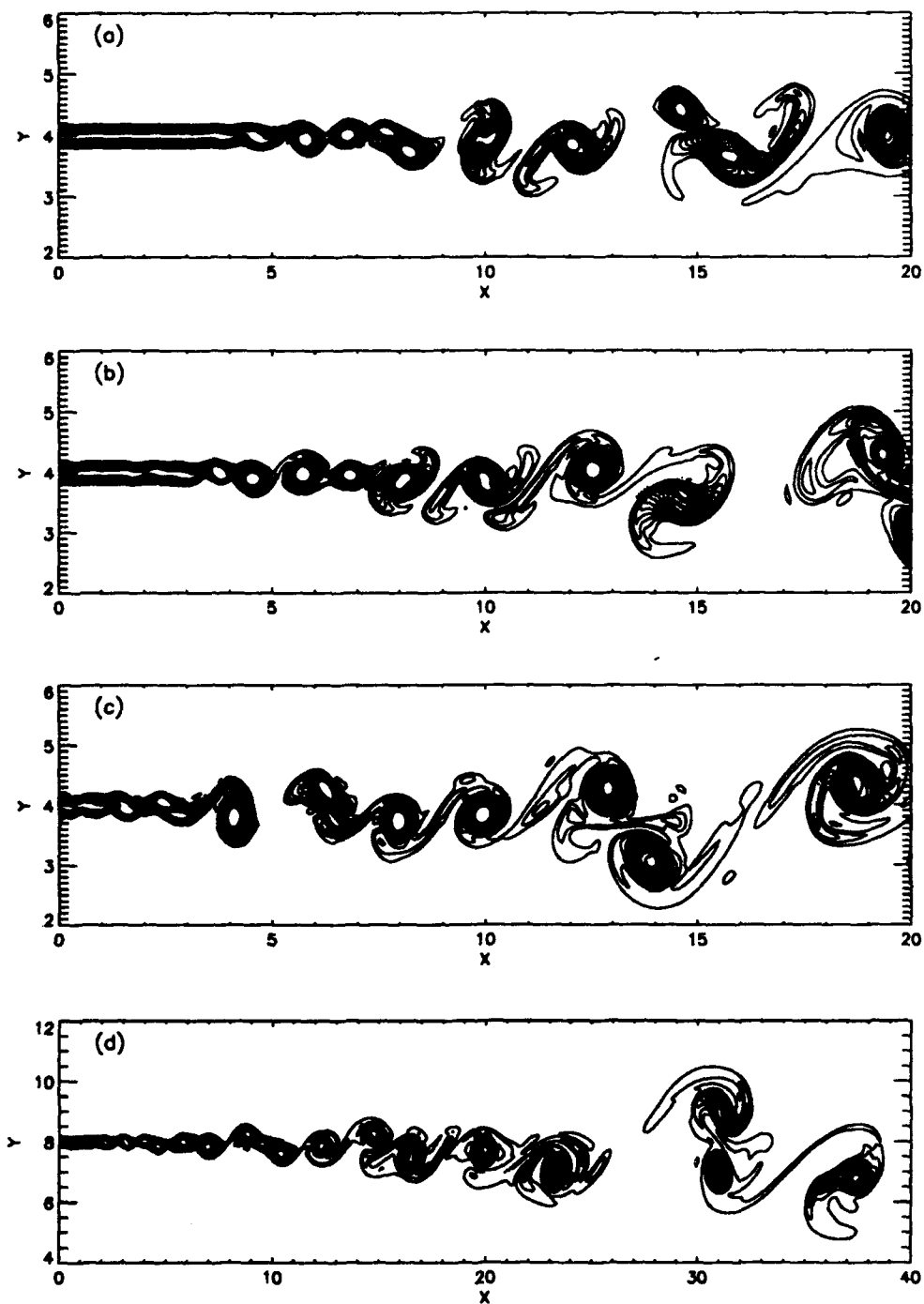**FIG. 4.** Vorticity contours from fundamental mode simulation at $t = 2.708$, $Re = 10^2$.
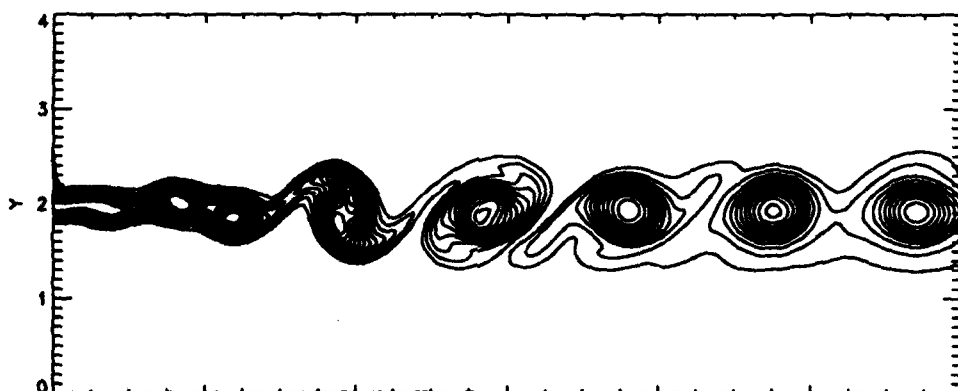


**FIG. 5.** Vorticity contours from fundamental/first subharmonic mode simulation at $t = 2.708$, $Re = 10^2$.
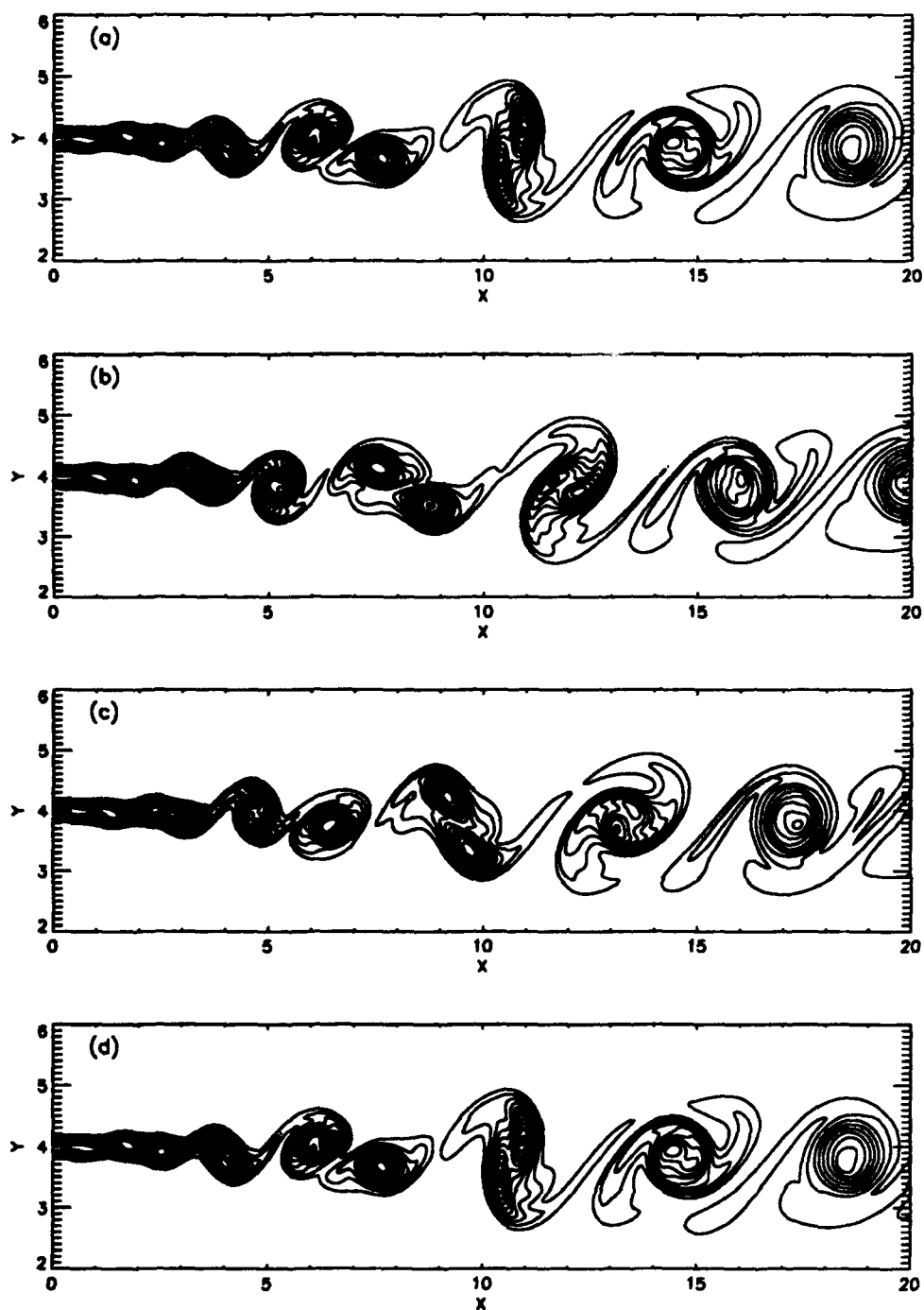
FIG. 6.    Vorticity contours from fundamental, first and second subharmonic mode simulation at, (a) $t = 1.625$, (b) $t = 1.690$, (c) $t = 1.755$, (d) $t = 1.820$, $Re = 10^2$.

FIG. 7.    Vorticity contours from broad mode simulations, $t = 3.413$, $L = 20$,
$(u_{rms}/\Delta u)_{max} = $ ; (a) 0.0015, (b) 0.015, (c) 0.15, (d) $t = 1.625$, $L = 40$,
$(u_{rms}/\Delta u)_{max} = 0.015$, $Re = 10^2$.

34

**FIG. 8.** Vorticity contours from broad mode simulations, $t = 3.413$, $L = 20$, $(u_{rms}/\Delta u)_{max} =$; (a) 0.0015, (b) 0.015, (c) 0.15, (d) $t = 1.625$, $L = 40$, $(u_{rms}/\Delta u)_{max} = 0.015$, $Re = 10^4$.

35
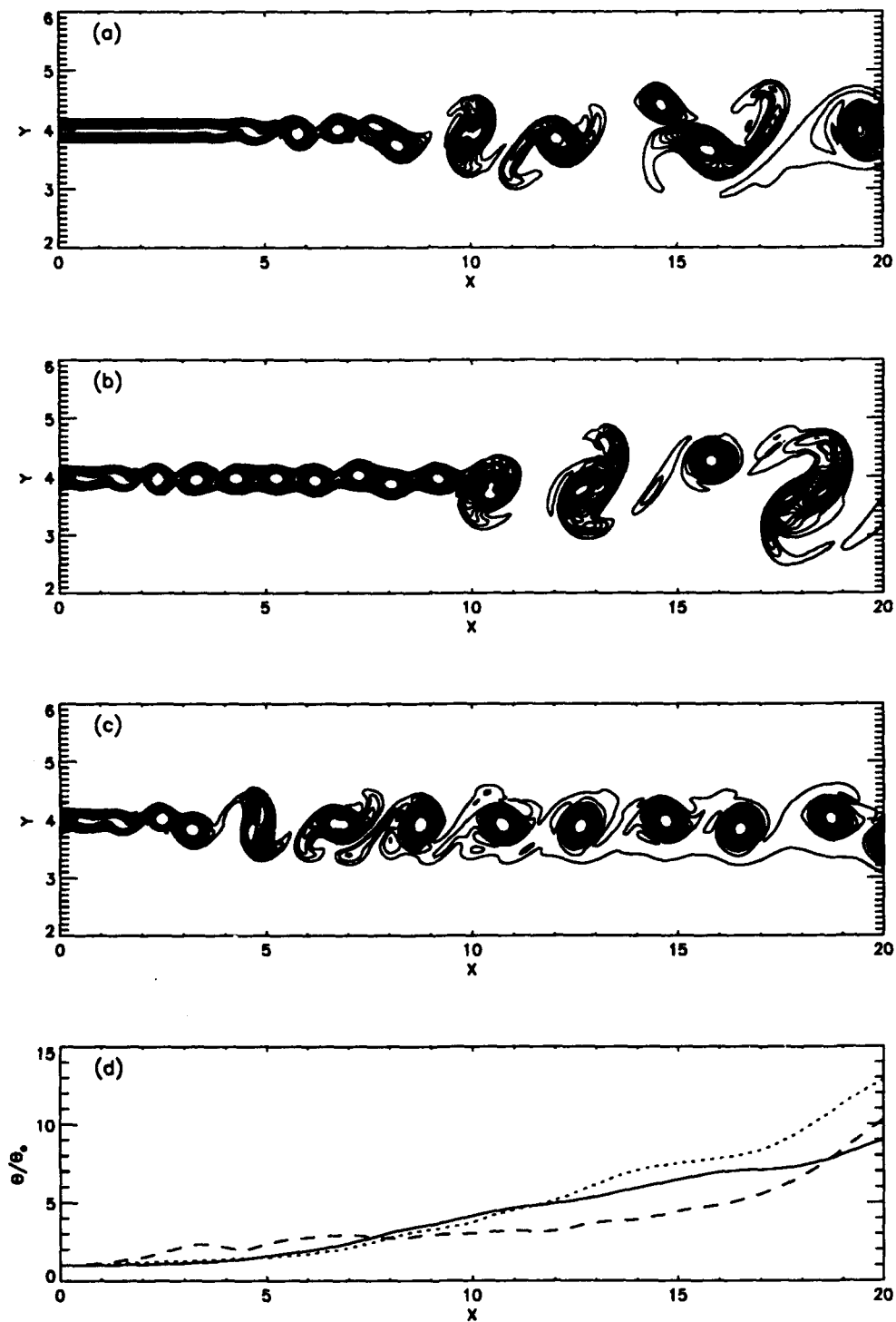
**FIG. 9**     Vorticity contours from simulations at $t = 3.413$, $L = 20$, forced with;
(a) broad mode only, (b) broad and fundamental modes, (c) broad, fundamental, and first subharmonic modes, (d) shear layer widths from (a) - (c),
————— : case (a) ; ⋯⋯⋯⋯ : case (b) ; – – – – : case (c), $Re = 10^4$.
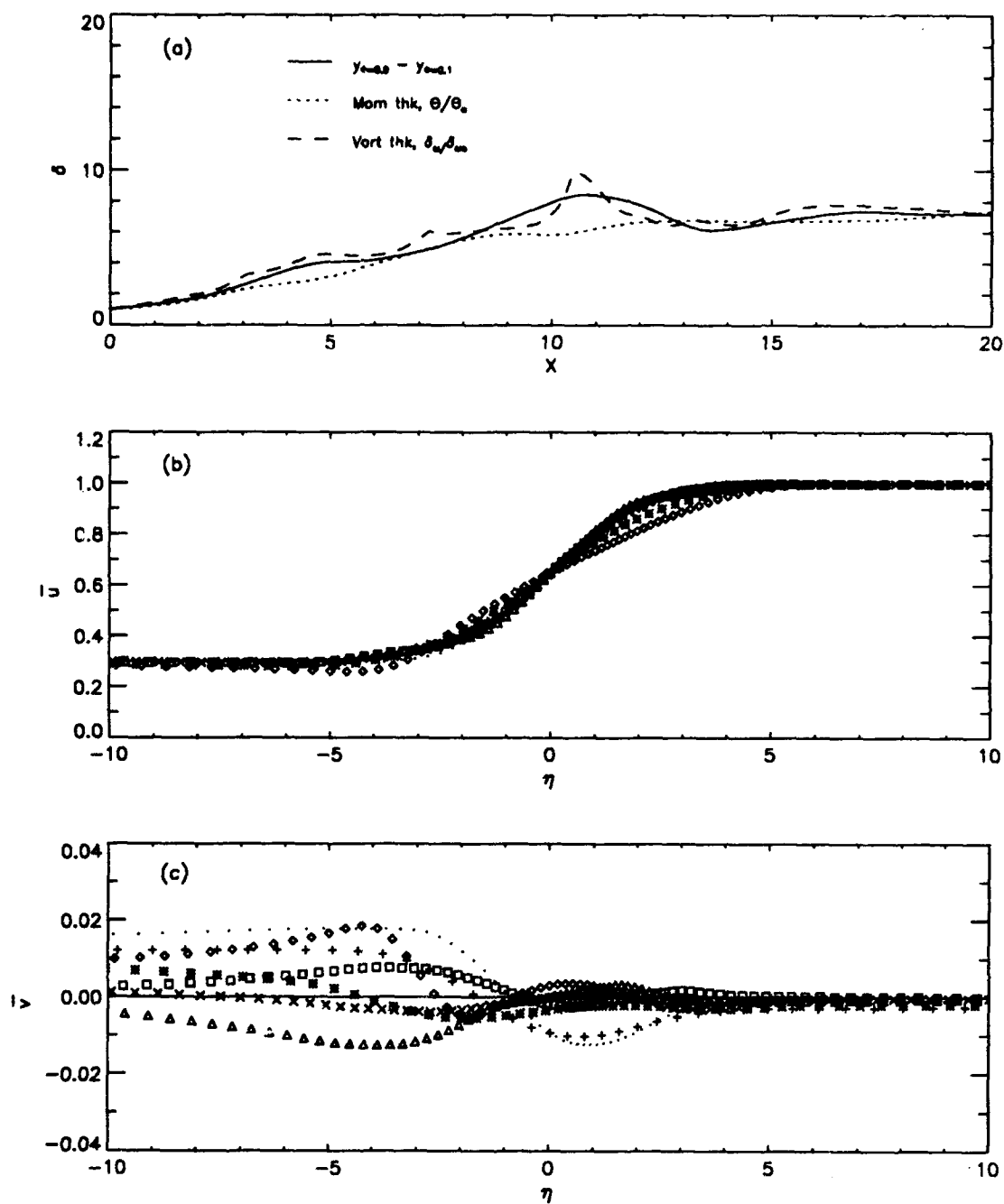
FIG. 10. Time-averaged properties from 3 mode simulation, distance from inflow, $x =;$ —— : 0.0 ; + : 2.5 ; ✳ : 5.1 ; ... : 7.7 ; ◇ : 10.3 ; △ : 12.8 ; □ : 15.4 ; ✕ : 18.0 , $Re = 10^2$.
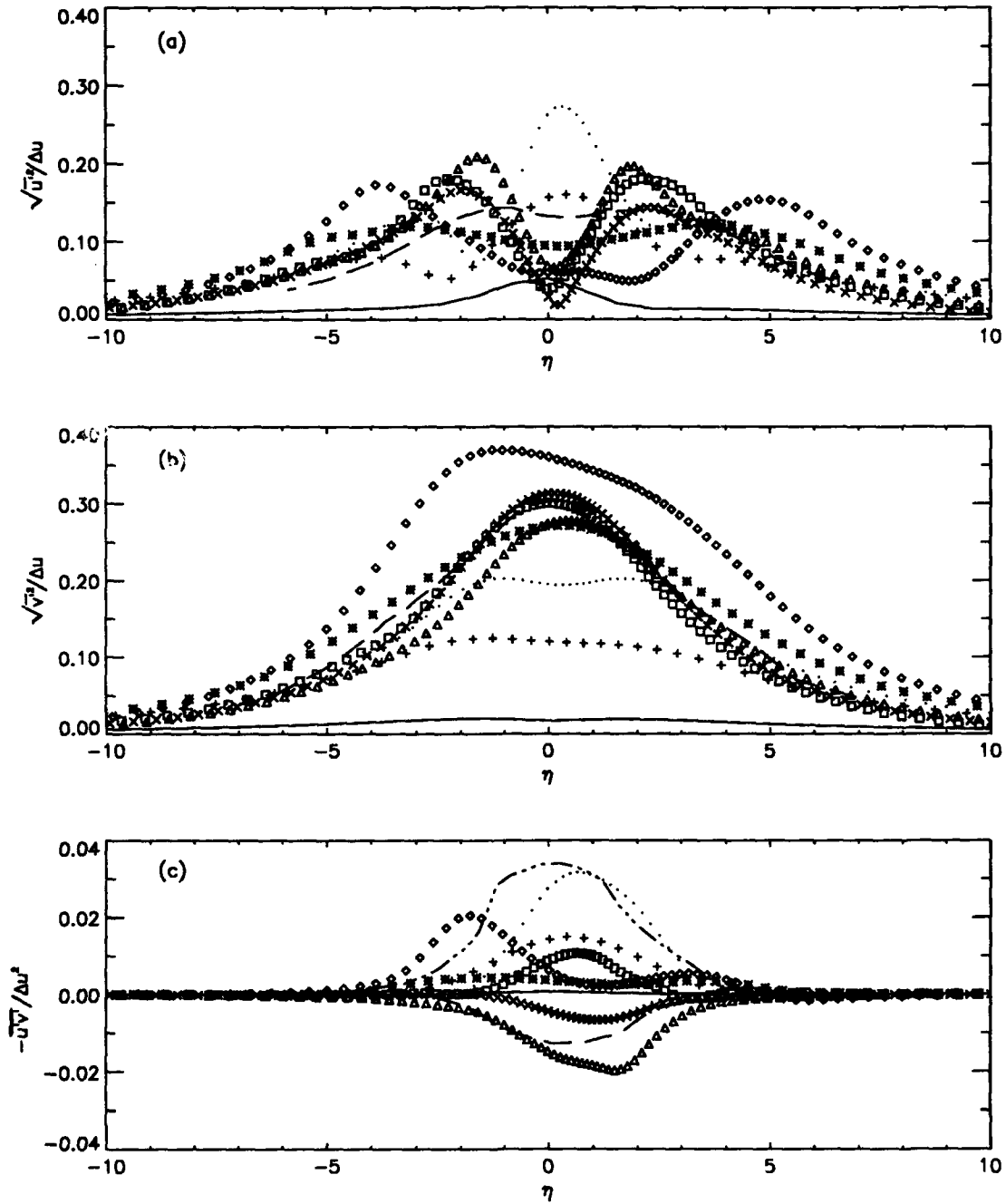
FIG. 11. Time-averaged properties from 3-mode simulation,

— — — : Oster and Wygnanski[26] (Forced, region of no vortex pairing),

—•••— : Oster and Wygnanski[26] (Forced, region of vortex pairing), (c) only;

$Re = 10^2$. For legend see Fig. 9.
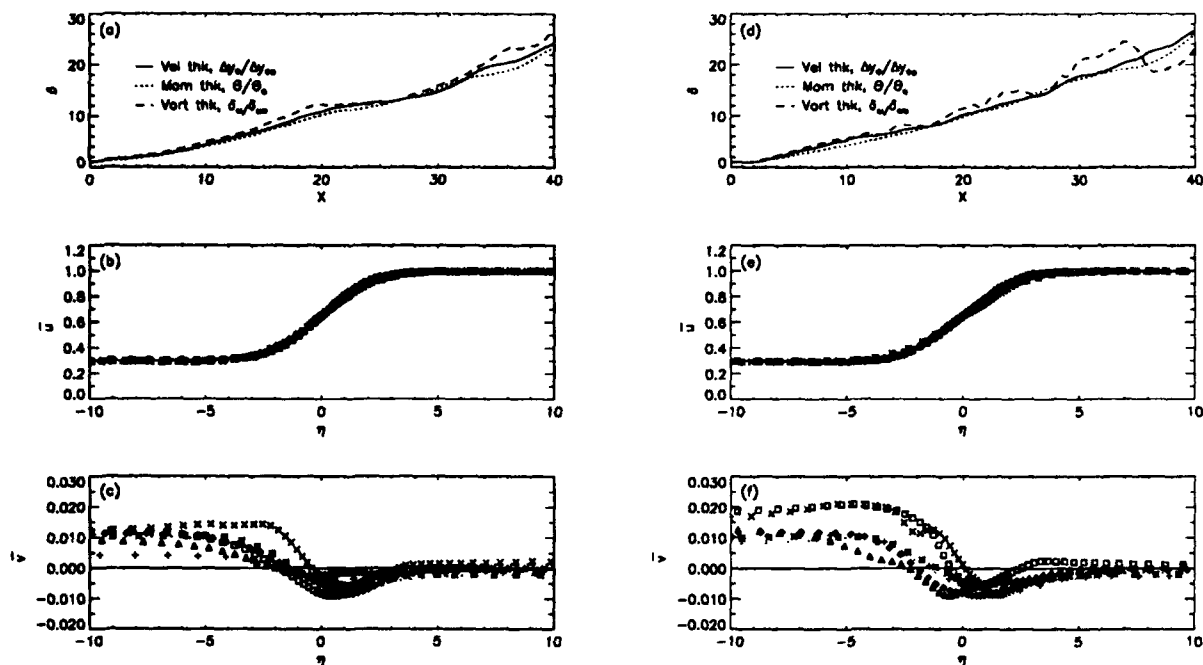
**FIG. 12.** Time-averaged properties from broad mode simulation, (a) - (c) $Re = 10^2$, (d) - (f) $Re = 10^4$, distance from inflow, $x =$; ——— : 0.0 ; $+$ : 9.2 ; $\ast$ : 13.5 ; ... : 17.8 ; $\diamondsuit$ : 22.1 ; $\triangle$ : 26.4 ; $\square$ : 30.7 ; $\times$ : 35.0.
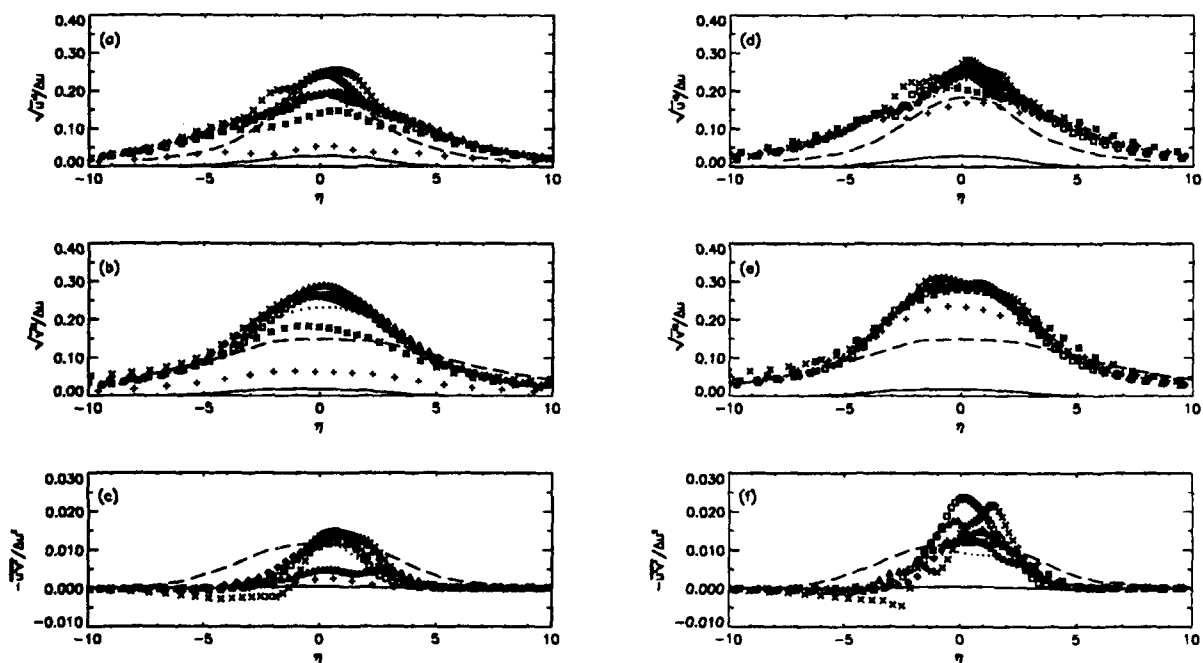


**FIG. 13.** Time-averaged properties from broad mode simulation,
— — — : Oster and Wygnanski[26] (Unforced, naturally-developing layer).
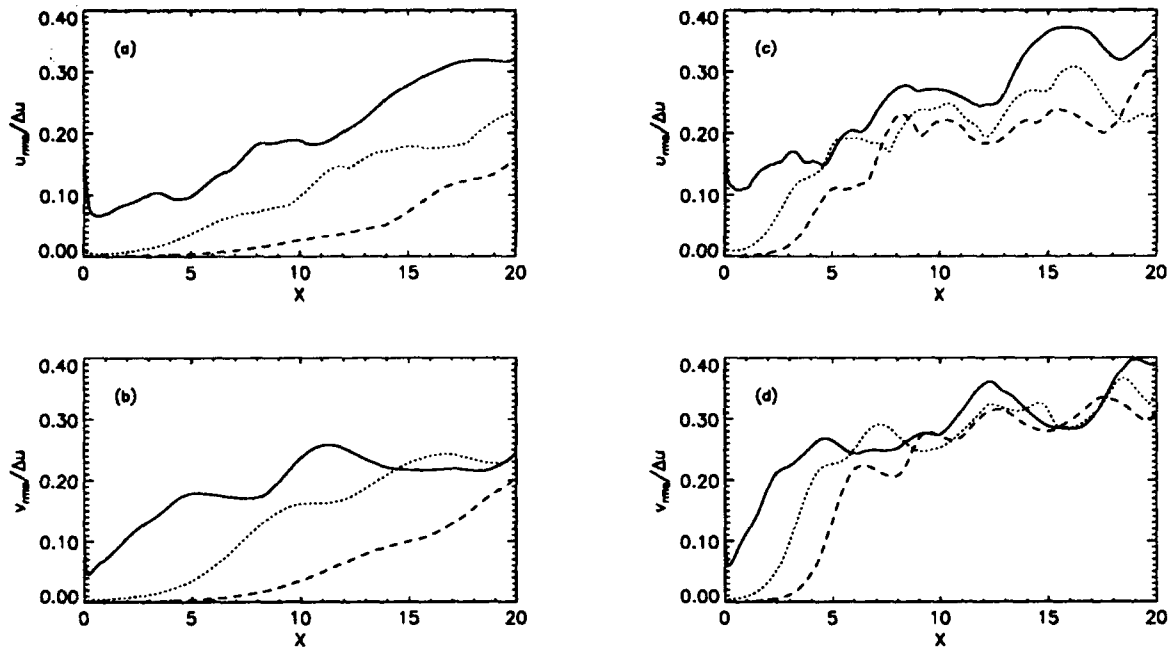For legend see Fig. 11.

39

FIG. 14.    Streamwise development of $u_{rms}$ and $v_{rms}$, $L = 20$,

(a) - (b) $Re = 10^2$, (c) - (d) $Re = 10^4$,  $(u_{rms}/\Delta u)_{max} =$;

———— : 0.15; ·······: 0.015 ; – – – – : 0.0015.
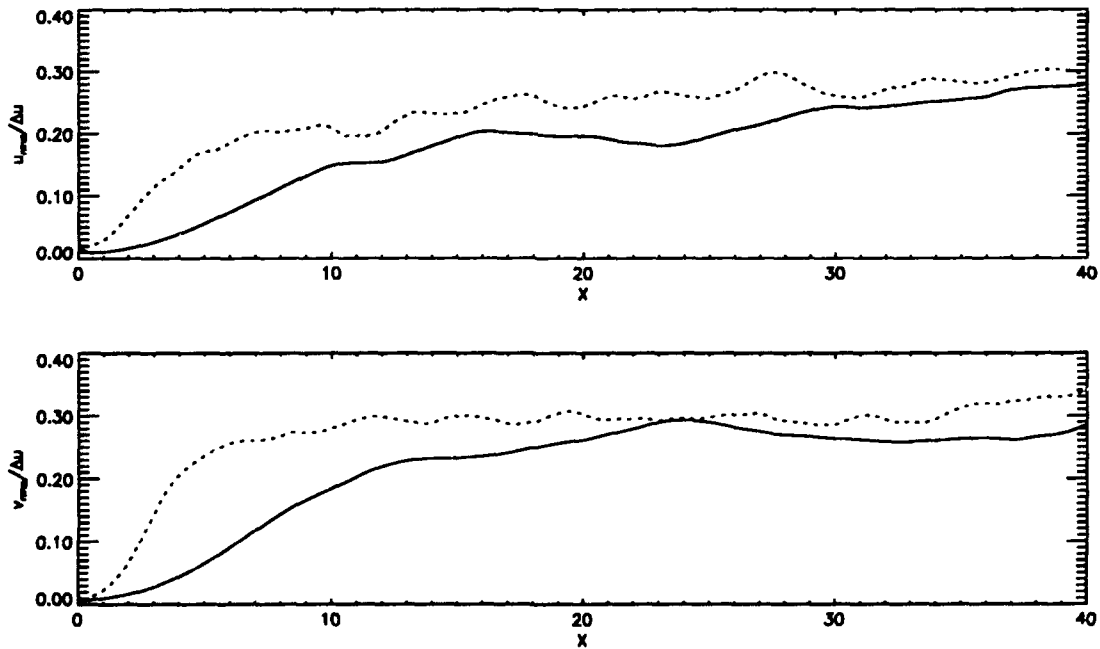


FIG. 15.    Streamwise development of $u_{rms}$ and $v_{rms}$, $L = 40$,

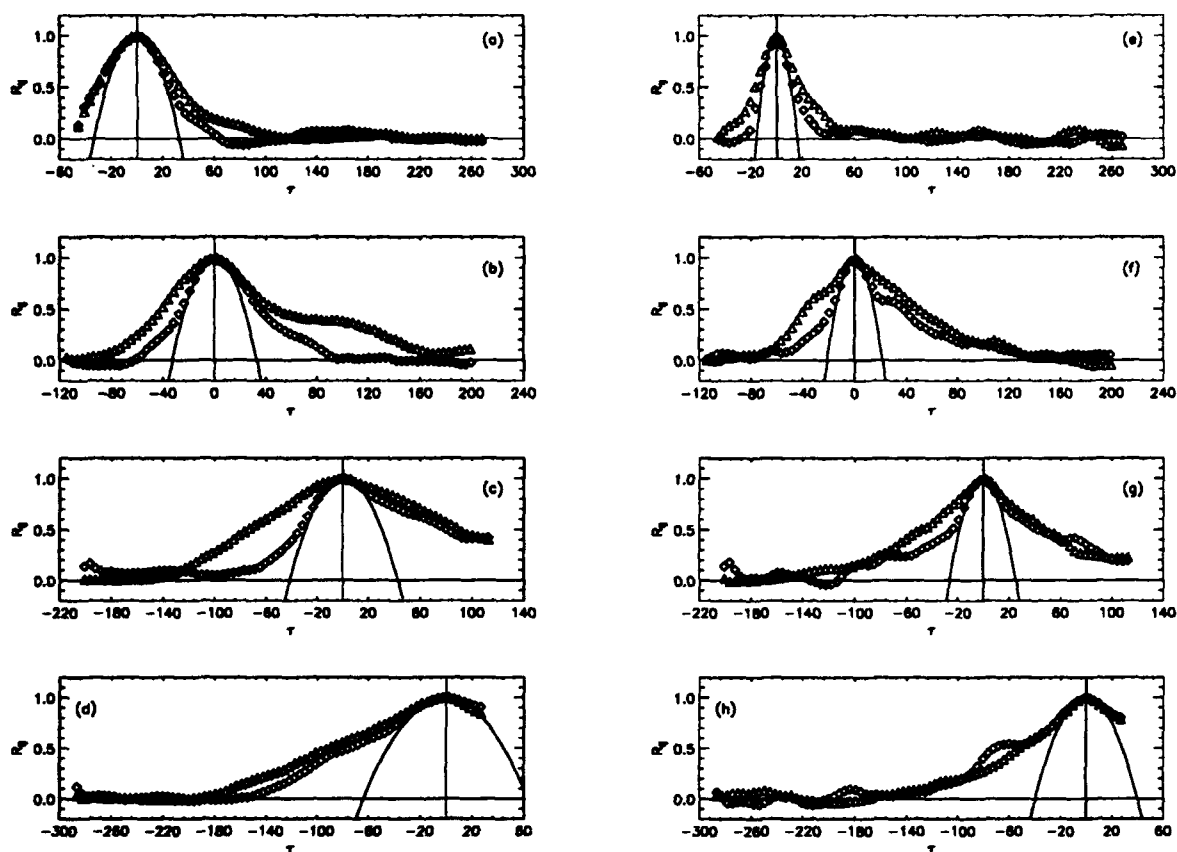———— : $Re = 10^2$ ; ·······: $Re = 10^4$,  $(u_{rms}/\Delta u)_{max} = 0.015$.

40

FIG. 16. $R_{11}$ ($\diamond$) and $R_{22}$ ($\triangle$) autocorrelations, (a) - (e) $Re = 10^2$, (f) - (j) $Re = 10^4$, at streamwise location, $x_o =$ ; (a), (f) 2.9, (b), (g) 5.7, (c), (h) 14.3, (d), (i) 25.2, (e), (j) 36.0, —— : 2nd degree curve fit of $R_{ij}$ at $\tau = 0$.
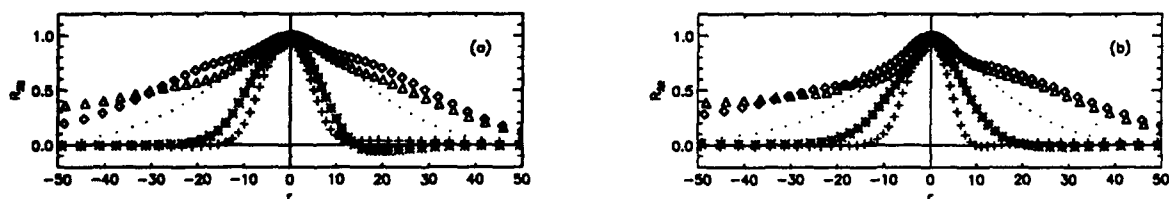


FIG. 17. $R_{22}$ two-point spatial correlations, (a) $Re = 10^2$, (b) $Re = 10^4$, at streamwise location, $x_o =$ ; $+$ : 2.9 ; $\divideontimes$ : 5.7 ; . . . : 14.3 ; $\diamond$ : 25.2 ; $\triangle$ : 36.0.

41

# REPORT DOCUMENTATION PAGE

Public reporting burden for this collection of information is estimated to average 1 hour per response, including the time for reviewing instructions, searching existing data sources, gathering and maintaining the data needed, and completing and reviewing the collection of information. Send comments regarding this burden estimate or any other aspect of this collection of information, including suggestions for reducing this burden, to Washington Headquarters Services, Directorate for Information Operations and Reports, 1215 Jefferson Davis Highway, Suite 1204, Arlington, VA 22202-4302, and to the Office of Management and Budget, Paperwork Reduction Project (0704-0188), Washington, DC 20503.

| 1. AGENCY USE ONLY(Leave blank) | 2. REPORT DATE May 1994 | 3. REPORT TYPE AND DATES COVERED Contractor Report |
|---|---|---|

**4. TITLE AND SUBTITLE**
NUMERICAL SIMULATION OF TWO-DIMENSIONAL SPATIALLY-DEVELOPING MIXING LAYERS

**5. FUNDING NUMBERS**
C NAS1-19480
WU 505-90-52-01

**6. AUTHOR(S)**
R.V.Wilson and A.O.Demuren

**7. PERFORMING ORGANIZATION NAME(S) AND ADDRESS(ES)**
Institute for Computer Applications in Science
and Engineering
Mail Stop 132C, NASA Langley Research Center
Hampton, VA 23681-0001

**8. PERFORMING ORGANIZATION REPORT NUMBER**
ICASE Report No. 94-32

**9. SPONSORING/MONITORING AGENCY NAME(S) AND ADDRESS(ES)**
National Aeronautics and Space Administration
Langley Research Center
Hampton, VA 23681-0001

**10. SPONSORING/MONITORING AGENCY REPORT NUMBER**
NASA CR-194911
ICASE Report No. 94-32

**11. SUPPLEMENTARY NOTES**
Langley Technical Monitor: Michael F. Card
Final Report
Submitted to Physics of Fluids

**12a. DISTRIBUTION/AVAILABILITY STATEMENT**

Unclassified–Unlimited

Subject Category 34

**12b. DISTRIBUTION CODE**

**13. ABSTRACT** (Maximum 200 words)

Two-dimensional, incompressible, spatially developing mixing layer simulations are performed at $Re = 10^2$ and $10^4$ with two classes of perturbations applied at the inlet boundary; (i) combinations of discrete modes from linear stability theory, and (ii) a broad spectrum of modes derived from experimentally measured velocity spectra. The effect of the type and strength of inlet perturbations on vortex dynamics and time-averaged properties are explored. Two-point spatial velocity and autocorreltations are used to estimate the size and lifetime of the resulting coherent structures and to explore possible feedback effects. The computed time-averaged properties such as mean velocity profiles, turbulent statistics, and spread rates show good agreement with experimentally measured values. It is shown that by forcing with a broad spectrum of modes derived from an experimental energy spectrum many experimentally observed phenomena can be reproduced by a 2-D simulation. The strength of the forcing merely affected the length required for the dominant coherent structures to become fully-developed. Thus intensities comparable to those of the background turbulence in many wind tunnel experiments produced the same results, given sufficient simulation length.

| 14. SUBJECT TERMS Mixing layers, numerical simulation, spatial simulation | 15. NUMBER OF PAGES 45 |
|---|---|
| | 16. PRICE CODE A03 |

| 17. SECURITY CLASSIFICATION OF REPORT Unclassified | 18. SECURITY CLASSIFICATION OF THIS PAGE Unclassified | 19. SECURITY CLASSIFICATION OF ABSTRACT | 20. LIMITATION OF ABSTRACT |
|---|---|---|---|

☆U.S. GOVERNMENT PRINTING OFFICE: 1994 - 528-064/23002